

# Combined Quantitative Assessment of Myocardial Perfusion and Coronary Artery Calcium Score by Hybrid $^{82}\text{Rb}$ PET/CT Improves Detection of Coronary Artery Disease

Yafim Brodov<sup>1</sup>, Heidi Gransar<sup>1</sup>, Damini Dey<sup>1,2</sup>, Aryeh Shalev<sup>1</sup>, Guido Germano<sup>1,2</sup>, John D. Friedman<sup>1</sup>, Sean W. Hayes<sup>1</sup>, Louise E.J. Thomson<sup>1</sup>, André Rogatko<sup>3</sup>, Daniel S. Berman<sup>1,2</sup>, and Piotr J. Slomka<sup>1,2</sup>

<sup>1</sup>Department of Imaging, Cedars-Sinai Medical Center, Los Angeles, California; <sup>2</sup>David Geffen School of Medicine, University of California Los Angeles, Los Angeles, California; and <sup>3</sup>Samuel Oschin Comprehensive Cancer Institute, Los Angeles, California

Hybrid PET myocardial perfusion imaging (MPI) with CT allows the incorporation of coronary artery calcium (CAC) into the clinical protocol. We aimed to determine whether the combined analysis of MPI and CAC could improve the diagnostic accuracy of PET MPI in detection of obstructive coronary artery disease (CAD).

**Methods:** Consecutive patients ( $n = 152$ ; mean age  $\pm$  SD,  $69 \pm 12$  y) without prior CAD, referred to  $^{82}\text{Rb}$  PET MPI followed by invasive coronary angiography performed within 14 days, were studied. Myocardial perfusion was quantified automatically for left anterior descending, left circumflex, and right coronary artery territories as an ischemic total perfusion deficit (ITPD) for 456 vessels. Global and per-vessel CAC Agatston scores were calculated. Obstructive CAD was defined as 50% or greater stenosis of the left main and 70% or greater stenosis in the left anterior descending, left circumflex, and right coronary arteries. Logistic regression and 10-fold cross validation were used to derive and validate the combined ITPD/logCAC (logarithm of coronary calcium) scores.

**Results:** In the prediction of per-vessel obstructive CAD, the receiver-operating-characteristic area under the curve for combined per-vessel ITPD/logCAC score was higher, 0.85 (95% confidence interval [CI], 0.81–0.89), than standalone ITPD area under the curve, 0.81 (95% CI: 0.76–0.85), and logCAC score, 0.73 (95% CI, 0.68–0.78;  $P < 0.05$ ). The integrated discrimination improvement of combined per-vessel ITPD/logCAC analysis was 0.07 (95% CI, 0.04–0.09;  $P < 0.0001$ ), as compared with ITPD alone. **Conclusion:** Combined automatically derived per-vessel ITPD and logCAC score improves accuracy of  $^{82}\text{Rb}$  PET MPI for detection of obstructive CAD.

**Key Words:** hybrid cardiac positron emission tomography; coronary calcium score; detection of obstructive coronary artery disease

J Nucl Med 2015; 56:1345–1350

DOI: 10.2967/jnumed.114.153429

**P**ET myocardial perfusion imaging (MPI) is a well-established noninvasive procedure for the evaluation and risk stratification of patients with coronary artery disease (CAD) (1–8). A principal advantage of hybrid PET combined with CT, compared with SPECT, is its potential ability to evaluate the coronary atherosclerotic burden as assessed by the coronary artery calcium (CAC) score during the PET scan. It is well known that many of the patients undergoing MPI have subclinical atherosclerosis, whereas at the same time a substantial proportion of patients may have a CAC score of 0 (9). Although the patients with abnormal MPI results can be defined as having CAD without CAC scan, the knowledge of the presence and extent of underlying coronary atherosclerosis could be useful in guiding therapeutic decisions especially in those with equivocal or mildly abnormal MPI studies. Moreover, CAC score is usually considered a global marker of atherosclerosis (10), and the regional CAC scores have been shown to improve the accuracy in detection of CAD (11). Ischemic total perfusion deficit (ITPD), which is a measure of hypoperfusion change between stress and rest in the whole ventricle (12), and CAC may be evaluated regionally, whereas the absolute quantitative measurements for both could be obtained readily by image analysis software for different vascular territories. In this work, we sought to test the hypothesis that the combination of regional ITPD (quantitative measure of the relative decrease in counts by vascular territory as compared with a normal database) along with regional and global CAC scores could enhance the overall diagnostic value of PET/CT in the detection of obstructive CAD.

## MATERIALS AND METHODS

### Patients

From consecutive patients undergoing  $^{82}\text{Rb}$  PET/CT MPI at Cedars Sinai Medical Center between January 2008 and September 2012 ( $n = 3,515$ ), we excluded those with known CAD (myocardial infarction, percutaneous coronary intervention, or coronary bypass surgery [ $n = 1,416$ ]), those with invasive coronary angiography greater than 6 mo of indexed PET MPI ( $n = 1,884$ ), and those who had no CAC scan at the time of PET/CT imaging ( $n = 63$ ). All selected patients ( $n = 152$ ) had no cardiac events in the interval between MPI and invasive coronary angiography. Clinical and demographic data were collected during patient interviews before the scanning. All patients provided written informed consent for the use of their clinical and imaging data for research purposes. Pretest likelihood for having CAD was calculated as previously described (13).

Received Dec. 22, 2014; revision accepted Jun. 2, 2015.

For correspondence or reprints contact: Piotr J. Slomka, Artificial Intelligence in Medicine Program, 8700 Beverly Blvd., Ste. A047N, Los Angeles, CA 90048.

E-mail: piotr.slomka@cshs.org

Published online Jul. 9, 2015.

COPYRIGHT © 2015 by the Society of Nuclear Medicine and Molecular Imaging, Inc.

## Imaging and Analysis Protocols

A detailed description of PET MPI/CAC imaging protocols and perfusion deficit quantitation is provided in the supplemental materials (available at <http://jnm.snmjournals.org>). Briefly, the patients underwent same-day rest–stress gated  $^{82}\text{Rb}$  PET MPI and CAC imaging on a hybrid Biograph 64 PET/CT scanner (Siemens) (14). A 6-min rest electrocardiogram-gated acquisition was started immediately before the injection of 925–1,850 MBq (25–50 mCi) of  $^{82}\text{Rb}$ . Pharmacologic stress was performed using intravenous adenosine infusion (15) or regadenoson bolus (16) in 99 and 53 patients, respectively. No adjunctive exercise was performed. A 6-min stress electrocardiogram-gated acquisition was started immediately with the  $^{82}\text{Rb}$  injection of 925–1,850 MBq (25–50 mCi). CT attenuation-correction scans were acquired for both stress and rest studies. After completion of PET MPI, without moving patients from the scan table, CAC scanning was performed. CAC scanning consisted of 30–40 slices encompassing the heart from the carina to the apex, with a 30- to 35-cm field of view sufficient to include the entire heart as well as the ascending and descending thoracic aorta. Radiation doses from  $^{82}\text{Rb}$  PET and CAC ranged between 1.8 and 3.8 mSv and 0.7 and 1.2 mSv, respectively.

Left-ventricular segmentation for PET images was performed as recently described (17). For regional analysis, the myocardial wall division into vascular territories was performed according to the 17-segment model of the American Heart Association (18). An abnormality threshold of 3.0 mean absolute deviations ( $\sim 2.5$  SDs) below the normalized counts of subjects in the normal reference database was applied to estimate the local extent of hypoperfusion in polar map coordinates. The perfusion defect extent was calculated as the percentage of the total surface area of the left ventricle for which test data were below the abnormality threshold. The quantitative perfusion variable used was total perfusion deficit (TPD), which reflects a combination of both defect severity and the extent of the defect as recently validated for  $^{82}\text{Rb}$  PET perfusion analysis (17). Per-vessel and global (per-patient) ITPD was defined as stress TPD – rest TPD, computed separately for each vascular territory—left anterior descending (LAD), left circumflex (LCX), and right coronary artery (RCA)—and for the entire left ventricle. Standard per-vessel Agatston CAC scores and global (per-patient) CAC scores were calculated (19). The CAC score for LAD was calculated as the sum of CAC score of the left main (LM) and LAD. The CAC score for LCX was the sum of CAC scores of LM and LCX. The same CAC categories of 0, 1–99, 100–399, and 400 or greater were used for per-patient and per-vessel measures of the severity of coronary calcifications.

## Invasive Coronary Angiography

Clinically indicated invasive coronary angiography was performed according to standard clinical protocols (mean time difference,  $14 \pm 27$  days; range, 0–170 days) after the PET/CT MPI. Coronary angiograms were visually analyzed and reported by 2 experienced interventional cardiologists. A stenosis of 50% or greater of luminal diameter of the LM or 70% or greater in the LAD, LCX, and RCA was considered to signify obstructive CAD. Diagonal lesions were considered as LAD, obtuse marginal and ramus arteries were considered as LCX, and posterior descending and posterolateral branches were considered as RCA.

## Statistical Analysis

All continuous variables were described as mean  $\pm$  SD. A student 2-sample *t* test and  $\chi^2$  test were used to compare the differences in continuous and categorical variables, respectively. All tests of hypothesis were 2-sided, with a critical significance level of 5%. The natural logarithm of CAC score (logCAC) was used because of a wide range of the CAC scores. Multivariable logistic regression was used to

develop an integrated (ITPD/logCAC) quantitative score predicting obstructive CAD. The first combined model used per-vessel ITPD/per-vessel logCAC, and the second model used per-vessel ITPD/per-patient logCAC. The prediction of obstructive CAD by the models was compared with the prediction by ITPD alone, as previously reported (17). A 10-fold cross-validation (CV) technique (20) that ensured that none of the image data creating the logistic regression model were used in the subsequent evaluation of the diagnostic performance of the same model was applied. To further clarify, in 10-fold CV each of the 10 models was built from approximately 90% of the 456 vessels—that is, from 410 vessels—and was then tested in the remaining 46 vessels. This procedure was repeated 10 times, each time leaving out a different 10% of the vessels for testing. Thus, for each procedure the specific model was tested only in unseen vessels, but there were 10 separate models. In our implementation of the 10-fold CV, the patients' arteries were always clustered at the patient level; thus, in each-fold of the CV, there were no patient data for which one artery belonged to the training set and the other artery of the same patient to the validation set. The procedure was performed in this manner to ensure the real-life test of the application, in which the method is tested always in new patients and no single patient is used in the training and validation at the same time. 10-fold CV has been definitively shown to have the smaller bias for discriminant analysis than other methods, such as split-sample, as traditionally used (20), in which just 1 arbitrary division into test and validation groups is performed. Receiver-operating-characteristic area-under-the-curve (AUC) analysis (21) and integrated discrimination improvement (IDI) (22) were applied to evaluate the discrimination ability of relevant predictors. IDI was defined as the difference between the integral of test sensitivity (IS) over all possible cutoff values from the (0, 1) interval and the

**TABLE 1**  
Patient Demographics and Clinical Characteristics

Description	Value
Age (y)	69 $\pm$ 12
Male	94 (62%)
Body mass index (kg/m <sup>2</sup> )	28 $\pm$ 6
Diabetes	64 (42%)
Hypertension	115 (76%)
Hypercholesterolemia	93 (61%)
Smoking	24 (16%)
Left ventricular hypertrophy	10 (6%)
Significant valvular disease	4 (3%)
Typical angina	15 (10%)
Shortness of breath	74 (49%)
Low likelihood	0
Intermediate likelihood	44 (29%)
High likelihood	108 (71%)
Antiplatelet drugs	80 (53%)
Angiotensin-converting enzyme inhibitors	39 (26%)
$\beta$ -blockers	67 (44%)
Statins	77 (51%)

Values are mean  $\pm$  SD or number followed by percentage of total number of patients in parentheses.

**TABLE 2**  
Myocardial Perfusion Imaging and CAC Scan Findings

Finding	Per patient (n = 152)	Per vessel (n = 456)		
		LAD (n = 152)	LCX (n = 152)	RCA (n = 152)
Stress TPD	11.4 ± 10.6	5.3 ± 8.0	3.1 ± 3.9	3.8 ± 4.6
Rest TPD	2.2 ± 4.0	1.0 ± 3.0	0.6 ± 1.6	0.8 ± 1.9
ITPD	9.7 ± 8.7	4.3 ± 6.7	2.5 ± 3.1	3.0 ± 3.6
CAC score	923 ± 1212	430 ± 511	201 ± 356	339 ± 605
Stress LVEF	60 ± 17	—	—	—
Rest LVEF	59 ± 17	—	—	—

CAC score is expressed as mean ± SD in Hounsfield units; other values are percentage and mean ± SD.  
LVEF = left ventricular ejection fraction.

corresponding integral of 1 minus specificity (IP). Thus, the IDI is defined as follows:

$$IDI = (IS_{\text{new}} - IS_{\text{old}}) - (IP_{\text{new}} - IP_{\text{old}}).$$

The subscript new in the above expression refers to the model with the new marker, and subscript old refers to the model without it. Because the integrals of sensitivity and 1 minus specificity over the (0, 1) interval can be seen as average sensitivity and 1 minus specificity, the IDI can be viewed as a difference between improvement in average sensitivity and any increase in average 1 minus specificity. Statistical analyses were performed with STATA software (version 12; Stata Corp LP) and SAS software (version 9.2; SAS Institute Inc.).

## RESULTS

### Overall Characteristics

Baseline clinical features of the studied population are presented in Table 1. Angiographically normal/nonsignificant CAD and significant single-, double-, and triple-vessel CAD were present in 41%, 32%, 14%, and 13% of patients, respectively. Ten patients (6.6%) had significant LM disease: 2 patients had a combination of LM with triple-vessel disease, 5 had LM with double-vessel disease, and 3 had LM with single vessel disease. None had isolated significant LM disease. Chronic total occlusion of LAD, LCX, and RCA or their branches in 8, 5, and 17 patients, respectively, was seen. The therapeutic decisions were based on primarily visual assessment of coronary lumen in 437 vessels, but in 19 visually borderline vessels, fractional flow reserve analysis was used. Among 89 patients with a 70% or greater stenosis, immediate revascularization was recommended in 76 (85%). In another 13 patients (15%) with total chronic occlusions and good collateral flow to the territories supplied by occluded vessels, conservative management was considered.

A normal MPI result was observed in 24 (16%) patients. Mild-moderate reversible defects (ITPD 1%–9%) and significant reversible defects (ITPD ≥ 10%) were seen in 69 (45%) and 49 (32%) patients, respectively. Fixed perfusion defects—mild-moderate (stress TPD = rest TPD < 10%) and significant (stress TPD = rest TPD ≥ 10%)—were seen only in 7 (5%) and 3 patients (2%), respectively. CAC scores of 0, 1–99, 100–399, and 400 or greater in 14 (9%), 19 (13%), 40 (26%), and 79 (52%) patients, respectively, were seen. Scintigraphic and CAC findings are summarized in Table 2. Distributions of per-vessel ITPD categories across

different per-vessel CAC score categories are shown in Figure 1. Per-vessel analysis (n = 456) showed that the higher ITPD values were associated with the higher CAC (Fig. 1). Figure 2 illustrates the prevalence of obstructive CAD across different categories of ITPD and CAC. CAC, ITPD, and hypercholesterolemia were found to be independent predictors of obstructive CAD in multivariable analysis (Table 3).

### Diagnostic Performance of Combined Models

The logistic regression coefficients for combined models can be calculated using the following equations:

$$1/(1 + \text{Exp}(3.65 - 0.34 \times \text{per-vessel ITPD} - 0.39 \times \log(\text{per-vessel CAC} + 1))) \quad \text{Eq. 1}$$

$$1/(1 + \text{Exp}(4.44 - 0.34 \times \text{per-vessel ITPD} - 0.42 \times \log(\text{global CAC} + 1))) \quad \text{Eq. 2}$$

The logistic regression coefficients for both combined models are shown in Table 4. The Wald test was significant ( $P < 0.001$ ) for

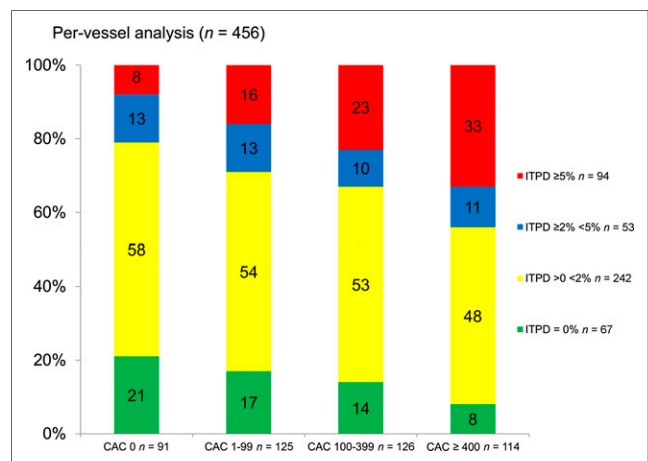


**FIGURE 1.** Distribution of ITPD categories according to CAC scores (per-vessel analysis, n = 456). Frequency of ITPD ≥ 5% (red bars) was significantly higher in vessels with CAC score > 400 than in others,  $P < 0.001$ . In contrast, frequency of ITPD = 0 (green bars) was significantly higher in vessels with CAC=0 scores than in others,  $P = 0.007$ .

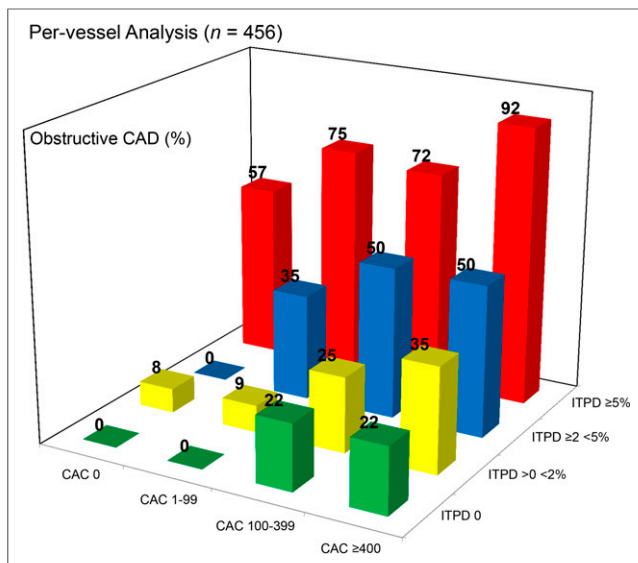


**FIGURE 2.** Prevalence of obstructive CAD across ITPD and CAC categories (per-vessel analysis,  $n = 456$ ). Among CAC = 0 vessels, risk of obstructive CAD was higher among ITPD  $\geq 5\%$  vessels (red bars) than others,  $P$  for trend = 0.0006. Moreover, among ITPD = 0 vessels (green bars), risk of obstructive CAD was still significantly higher in CAC  $\geq 400$  vessels than in others,  $P$  for trend 0.006.

both models. In the prediction of obstructive CAD, the AUC for per-vessel ITPD/logCAC combined scores (0.85; 95% confidence interval [CI], 0.81–0.89) was significantly higher than AUCs for per-vessel ITPD (0.81; 95% CI, 0.76–0.85) or per-vessel logCAC (0.73; 95% CI, 0.68–0.78;  $P = 0.02$  and  $<0.0001$ , respectively) (Figs. 3A and 3B, respectively). Table 5 shows IDI analysis for the prediction of obstructive CAD using both combined models. The lower 95% CIs of IDI are greater than 0 for individual-vessel analysis ( $n = 152$ ) and per-patient analysis ( $n = 152$ ). The cutoff threshold for the combined score 0.312 has been determined to match the sensitivity of the previously established MPI diagnostic threshold for per-vessel ITPD (2%) (17). On the basis of the receiver-operating-characteristic curve in Figure 3A, such a threshold

results in the overall specificity increase from 72% to 80%,  $P = 0.0009$ , maintaining the same sensitivity of 72% as achieved by ITPD alone. The clinical usefulness of combined analysis is shown in Supplemental Figures 4–6.

## DISCUSSION

We have shown that the computational integration of automatically derived perfusion parameters with a logCAC score obtained by hybrid  $^{82}\text{Rb}$  PET/CT MPI allows a more accurate per-vessel prediction of obstructive CAD than perfusion parameters alone. Prediction of obstructive CAD improved similarly when per-vessel and global logCAC scores were added to per-vessel ITPD. The similar additive value of per-vessel and per-patient logCAC scores demonstrates the nature of CAC findings, which likely reflect global risk for CAD rather than a presence of CAD in a given vessel, unlike MPI findings.

Several studies evaluated the additional value of CAC to MPI in the diagnosis of CAD. Schepis et al. (23) found that a CAC score of 709 or greater as a cutoff for detection of significant CAD was missed by MPI. Bybee et al. (6) studied patients without CAD and normal PET perfusion scans and found a high prevalence of significant subclinical atherosclerosis in 22% and 30% of patients who had CAC scores 100 or greater and 400 or greater, respectively. Thompson et al. (24) found 17% of normal perfusion studies were reclassified to have significant coronary atherosclerosis with a CAC score of 100 or greater. Ghadri et al. (25) demonstrated a high diagnostic value of CAC scores of 1,000 or greater for detecting CAD despite normal MPI. The additional prognostic value of CAC in adjunct to PET and SPECT MPI was also studied by Schenker et al. (9) and Chang et al. (26), demonstrating a step-wise increase in risk of adverse events with increasing CAC in patients with and without ischemia.

Although our study is in general agreement with the aforementioned studies, we derive a novel quantitative hybrid score. This score applies to any combination of ITPD and CAC values, in contrast to previously proposed CAC thresholds (6,25). Consequently, the developed technique allows us to demonstrate the increase in the overall diagnostic performance of hybrid PET/CAC in consecutive patients referred to clinically indicated MPI for suspected CAD. We analyzed perfusion abnormalities and

**TABLE 3**  
Univariate and Multivariable Imaging and Clinical Predictors of Obstructive CAD ( $n = 152$ )

Predictor	Univariate analysis			Multivariable analysis		
	OR	95% CI	<i>P</i>	OR	95% CI	<i>P</i>
logCAC	1.49	1.24–1.78	$<0.001$	1.40	1.10–1.77	0.006
ITPD	1.28	1.17–1.40	$<0.001$	1.29	1.17–1.42	$<0.001$
Age	1.04	1.01–1.06	0.02	1.01	0.96–1.05	0.76
Pretest likelihood	1.01	1.00–1.03	0.03	1.01	0.99–1.03	0.29
Male sex	1.04	0.54–2.03	0.90	—	—	—
Diabetes mellitus	1.06	0.55–2.04	0.86	—	—	—
Hypertension	1.01	0.47–2.16	0.98	—	—	—
Hypercholesterolemia	2.25	1.15–4.38	0.02	2.84	1.09–7.40	0.03

OR = odds ratio.

**TABLE 4**  
Odds Ratios and Coefficients for Logistic Regression Models from 10-Fold Cross Validation

Predictor	Per-vessel logCAC score			Global (per-patient) global logCAC score		
	OR	95% CI	Coefficients 10-CV (mean ± SE)	OR	95% CI	Coefficients 10-CV (mean ± SE)
ITPD	1.41	1.30–1.53	0.34 ± 0.02	1.41	1.30–1.52	0.34 ± 0.02
logCAC	1.47	1.29–1.67	0.39 ± 0.03	1.53	1.30–1.79	0.42 ± 0.04
Constant	—		−3.65 ± 0.12	—		−4.44 ± 0.22

OR = odds ratio.

CAC separately for every major artery, relating perfusion territory for calcium score in the artery supplying corresponding territory. In a related study, Schuijff et al. found a moderate correlation between regional CAC scores and regional ischemia (27).

Our work has important clinical implications. In patients with suspected CAD, the combined perfusion and CAC analysis improves the detection of obstructive CAD, supporting the routine application of such an approach. Because most current PET scanners have at least 16-slice CT, which is sufficient for CAC scoring, an additional CAC scan is easily accommodated by the hybrid  $^{82}\text{Rb}$  PET/CT MPI protocol (28). In addition, software techniques have been proposed for PET/CT, which can register a single CAC scan to PET for attenuation correction of stress and rest PET (29). Our study establishes the quantitative model for the optimal prediction of obstructive CAD, combining both PET and CAC scans. To facilitate a practical clinical deployment, this model (as given in Eqs. 1 and 2) could be integrated with the results obtained by the existing quantitative MPI software. Our study could not find a difference between the global and per-vessel CAC for this purpose. Larger studies may be needed to confirm the superiority of either approach. Incorporation of these hybrid scores to routine clinical reporting would allow objective improvement in the diagnoses provided by PET MPI.

The limitations of this study include that a small patient cohort from a single medical center was retrospectively analyzed, reflecting difficulties in obtaining correlating PET MPI, CAC, and invasive angiography data. Nevertheless, the use of 10-fold CV allowed for the construction of unbiased (20) logistic regression models trained on 90% fractions of the population. In addition, 10-fold CV allowed us to evaluate the model variability. As in many prior MPI studies with correlating invasive angiography, there is a referral bias (30). However, the goal of this study was to evaluate a relative improvement in the prediction of obstructive CAD with the combined approach, rather than to establish an absolute level of diagnostic accuracy of PET MPI. Quantitative coronary assessment was not performed in this study because angiography was visually estimated by 2 experienced interventional cardiologists. However, by our previous experience, these results are not significantly different from quantitatively established obstructive ( $\geq 70\%$ ) stenosis. In this study, we used ischemic measure (ITPD) and therefore did not consider the fixed defects; however, significant ( $>10\%$ ) fixed defects with unknown CAD were seen in only 3 patients (2%). Coronary flow reserve analysis was not used in our study, and it could potentially improve diagnostic accuracy; however, reduced flow reserve may be unrelated to obstructive

CAD. This work did not study patients with known CAD and therefore we cannot conclude if such combined analysis would have additional clinical value in this group. We did not consider the use of effect of statins on the results, and in our population 50% of the patients had been taking statins. Larger studies may be needed in the future to consider the effect of statins on CAC findings (31).

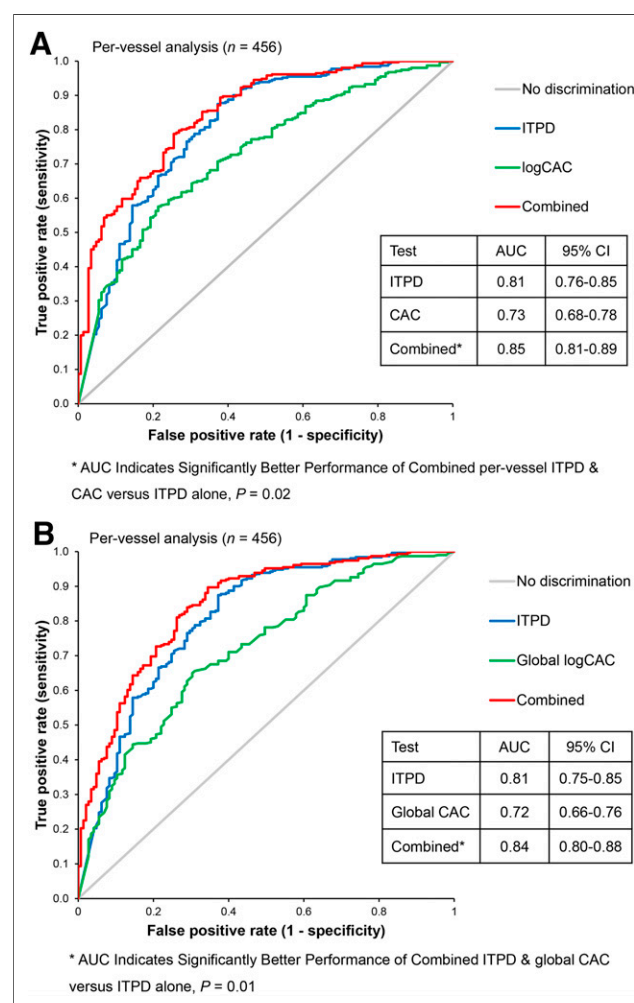


**FIGURE 3.** 10-fold cross-validated receiver-operating-characteristic analysis comparing combined performance of ITPD/logCAC vs. ITPD in predicting obstructive CAD. \*AUC of combined analysis ITPD with per-vessel (A) and global (B) CAC.

**TABLE 5**  
IDI Analysis

Combined models	IDI	P
ITPD/logCAC per patient (n = 152)	0.06 (0.01–0.10)	0.016
ITPD/logCAC per vessel (n = 456)	0.07 (0.04–0.09)	<0.0001
ITPD/logCAC for LAD (n = 152)	0.04 (0.00–0.07)	0.05
ITPD/logCAC for LCX (n = 152)	0.08 (0.03–0.13)	0.001
ITPD/logCAC for RCA (n = 152)	0.08 (0.04–0.13)	0.0003
ITPD/global logCAC (n = 456)	0.06 (0.04–0.08)	<0.0001

Data in parentheses are 95% CIs.

## CONCLUSION

Quantitative analysis integrating per-vessel ischemic TPD with logCAC scores synergistically improves the quantitative accuracy of  $^{82}\text{Rb}$  PET MPI for regional prediction of obstructive CAD.

## DISCLOSURE

The costs of publication of this article were defrayed in part by the payment of page charges. Therefore, and solely to indicate this fact, this article is hereby marked “advertisement” in accordance with 18 USC section 1734. Cedars-Sinai Medical Center receives royalties for the quantitative assessment of function, perfusion, and viability, a portion of which is distributed to some of the authors of this manuscript. Yafim Brodov, MD, PhD, is a Michael Kogan Save a Heart Foundation fellow in nuclear cardiology and cardiac imaging, Cedars Sinai Medical Center, Los Angeles, California. No other potential conflict of interest relevant to this article was reported.

## ACKNOWLEDGMENT

We thank Dr. Michael Pencina from Duke University for discussions regarding the AUC comparisons, for use of IDI, and for providing SAC macros for the IDI analysis.

## REFERENCES

1. Sampson UK, Dorbala S, Limaye A, Kwong R, Di Carli MF. Diagnostic accuracy of rubidium-82 myocardial perfusion imaging with hybrid positron emission tomography/computed tomography in the detection of coronary artery disease. *J Am Coll Cardiol*. 2007;49:1052–1058.
2. Murthy VL, Naya M, Foster CR, et al. Improved cardiac risk assessment with noninvasive measures of coronary flow reserve. *Circulation*. 2011;124:2215–2224.
3. Naya M, Murthy VL, Taqueti VR, et al. Preserved coronary flow reserve effectively excludes high-risk coronary artery disease on angiography. *J Nucl Med*. 2014;55:248–255.
4. Naya M, Murthy VL, Foster CR, et al. Prognostic interplay of coronary artery calcification and underlying vascular dysfunction in patients with suspected coronary artery disease. *J Am Coll Cardiol*. 2013;61:2098–2106.
5. Dorbala S, Vangala D, Sampson U, Limaye A, Kwong R, Di Carli MF. Value of vasodilator left ventricular ejection fraction reserve in evaluating the magnitude of myocardium at risk and the extent of angiographic coronary artery disease: a  $^{82}\text{Rb}$  PET/CT study. *J Nucl Med*. 2007;48:349–358.
6. Bybee KA, Lee J, Markiewicz R, et al. Diagnostic and clinical benefit of combined coronary calcium and perfusion assessment in patients undergoing PET/CT myocardial perfusion stress imaging. *J Nucl Cardiol*. 2010;17:188–196.

7. Morton G, Chiribiri A, Ishida M, et al. Quantification of absolute myocardial perfusion in patients with coronary artery disease: comparison between cardiovascular magnetic resonance and positron emission tomography. *J Am Coll Cardiol*. 2012;60:1546–1555.
8. Johnson NP, Gould KL. Physiological basis for angina and ST-segment change PET-verified thresholds of quantitative stress myocardial perfusion and coronary flow reserve. *JACC Cardiovasc Imaging*. 2011;4:990–998.
9. Schenker MP, Dorbala S, Hong EC, et al. Interrelation of coronary calcification, myocardial ischemia, and outcomes in patients with intermediate likelihood of coronary artery disease: a combined positron emission tomography/computed tomography study. *Circulation*. 2008;117:1693–1700.
10. Wong ND, Kouwabunpat D, Vo AN, et al. Coronary calcium and atherosclerosis by ultrafast computed tomography in asymptomatic men and women: relation to age and risk factors. *Am Heart J*. 1994;127:422–430.
11. Leschka S, Scheffel H, Desbiolles L, et al. Combining dual-source computed tomography coronary angiography and calcium scoring: added value for the assessment of coronary artery disease. *Heart*. 2008;94:1154–1161.
12. Slomka PJ, Nishina H, Berman DS, et al. Automated quantification of myocardial perfusion SPECT using simplified normal limits. *J Nucl Cardiol*. 2005;12:66–77.
13. Diamond GA, Forrester J. Analysis of probability as an aid in the clinical diagnosis of coronary-artery disease. *N Engl J Med*. 1979;300:1350–1358.
14. Blodgett TM, Meltzer CC, Townsend DW. PET/CT: form and function. *Radiology*. 2007;242:360–385.
15. Iskandrian AS, Verani MS, Heo J. Pharmacologic stress testing: mechanism of action, hemodynamic responses, and results in detection of coronary artery disease. *J Nucl Cardiol*. 1994;1:94–111.
16. Iskandrian AE, Bateman TM, Belardinelli L, et al. ADVANCE MPI Investigators. Adenosine versus regadenoson comparative evaluation in myocardial perfusion imaging: results of the ADVANCE phase 3 multicenter international trials. *J Nucl Cardiol*. 2007;14:645–658.
17. Nakazato R, Berman DS, Dey D, et al. Automated quantitative Rb-82 3D PET/CT myocardial perfusion imaging: normal limits and correlation with invasive coronary angiography. *J Nucl Cardiol*. 2012;19:265–276.
18. Cerqueira MD, Weissman N, Dilsizian V, et al. Standardized myocardial segmentation and nomenclature for tomographic imaging of the heart: a statement for healthcare professionals from the Cardiac Imaging Committee of the Council on Clinical Cardiology of the American Heart Association. *Circulation*. 2002;105:539–542.
19. Agatston AS, Janowitz WR, Hildner FJ, Zusmer NR, Viamonte M Jr, Detrano R. Quantification of coronary artery calcium using ultrafast computed tomography. *J Am Coll Cardiol*. 1990;15:827–832.
20. Molinaro AM, Simon R, Pfeiffer RM. Prediction error estimation: a comparison of resampling methods. *Bioinformatics*. 2005;21:3301–3307.
21. DeLong ER, DeLong DM, Clarke-Pearson DL. Comparing the areas under two or more correlated receiver operating characteristic curves: a nonparametric approach. *Biometrics*. 1988;44:837–845.
22. Pencina MJ, D’Agostino RB Sr, D’Agostino RB Jr, Vasan RS. Evaluating the added predictive ability of a new marker: from area under the ROC curve to reclassification and beyond. *Stat Med*. 2008;27:157–172.
23. Schepis T, Gaemperli O, Koepfli P, et al. Added value of coronary artery calcium score as an adjunct to gated SPECT for the evaluation of coronary artery disease in an intermediate-risk population. *J Nucl Med*. 2007;48:1424–1430.
24. Thompson RC, McGhie AI, Moser KW, et al. Clinical utility of coronary calcium scoring after nonischemic myocardial perfusion imaging. *J Nucl Cardiol*. 2005;12:392–400.
25. Ghadri JR, Pazhenkottal AP, Nkoulou RN, et al. Very high coronary calcium score unmasks obstructive coronary artery disease in patients with normal SPECT MPI. *Heart*. 2011;97:998–1003.
26. Chang SM, Nabi F, Xu J, et al. The coronary artery calcium score and stress myocardial perfusion imaging provide independent and complementary prediction of cardiac risk. *J Am Coll Cardiol*. 2009;54:1872–1882.
27. Schuijff JD, Wijns W, Jukema JW, et al. A comparative regional analysis of coronary atherosclerosis and calcium score on multislice CT versus myocardial perfusion on SPECT. *J Nucl Med*. 2006;47:1749–1755.
28. Mühlenbruch G, Klotz E, Wildberger JE, et al. The accuracy of 1- and 3-mm slices in coronary calcium scoring using multi-slice CT in vitro and in vivo. *Eur Radiol*. 2007;17:321–329.
29. Zaidi H, Nkoulou R, Bond S, et al. Computed tomography calcium score scan for attenuation correction of N-13 ammonia cardiac positron emission tomography: effect of respiratory phase and registration method. *Int J Cardiovasc Imaging*. 2013;29:1351–1360.
30. Rozanski A, Diamond GA, Berman DS, et al. The declining specificity of exercise radionuclide ventriculography. *N Engl J Med*. 1983;309:518–522.
31. Puri R, Nicholls SJ, Shao M. Impact of statins on serial coronary calcification during atheroma progression and regression. *J Am Coll Cardiol*. 2015;65:1273–1282.